Modeling of Microbial Dynamics and Geochemical Changes in a Metal Bioprecipitation Experiment

HENNING PROMMER,*,†
MICHELLE E. GRASSI,†,‡,§
ALEXANDER C. DAVIS,†,‡ AND
BRADLEY M. PATTERSON†

*CSIRO Land and Water, Private Bag No. 5,
Wembley WA 6913, Australia, Faculty of Life and Physical
Sciences, University of Western Australia, Western Australia*

A biogeochemical transport modeling study was carried out to analyze large-scale laboratory column experiments in which ethanol was used as an electron donor to create favorable conditions for the immobilization of selected trace metals (Zn and Cu) in groundwater. Microbial activity was explicitly simulated to capture the dynamic changes of the redox zonation within the column (i) in the early phase of the experiment (microbial lag) and (ii) in response to a significant decrease in the pH of the feed solution introduced after 188 days. The simulated redox dynamics agreed well with the observations after the pH-dependency of microbial growth was incorporated into the microbial model. The study showed that residual minerals may have buffered the pH for a period after the pH of the feed solution was decreased. Where the buffering capacity was exhausted, the pH decreased, leading to a successive downstream movement of the redox boundaries. The simulations reproduced the Zn immobilization within the sulfate-reducing zone as well as its partial remobilization after this zone moved further downstream. The immobilization of Cu within the denitrifying zone could also be well explained by incorporating malachite ($Cu_2(OH)_2CO_3$) precipitation in the simulations.

Introduction

The mobility of heavy metals in groundwater is strongly dependent on both the ambient pH and the prevailing redox conditions. Therefore, in situ manipulation (ISMP) of either acidity or redox conditions can be used to immobilize dissolved metals and significantly reduce their concentrations in the groundwater to below critical levels. To remediate metal-contaminated groundwater emanating from tailings dams, materials such as limestone, zerovalent iron, and organic carbon-rich material mixed with limestone have been used successfully as media in permeable reactive barriers (PRBs) [1, 2] that intercept acidic, metal-contaminated plumes [3–7]. Previous research suggests that metal removal in reactive barriers filled with easily oxidizable organic carbon predominantly relies on the ability of sulfate-reducing bacteria (SRB) to utilize organic carbon sources [3–6, 8–13]:

$$2CH_2O + SO_4 \rightarrow 2HCO_3^- + H_2S \qquad (1)$$

This oxidation of organic carbon by SRB creates an in situ reactive zone where metals may precipitate as metal sulfides:

$$Me^{2+} + H_2S \rightarrow MeS_{(solid)} + 2H^+ \qquad (2)$$
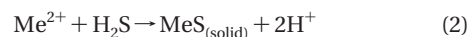
with Me^{2+} representing divalent metal cations. Alternatives to PRBs for delivering suitable carbon sources have been proposed [8, 10, 11, 14–16]. In contrast to PRBs, the direct injection of degradable organic carbon sources through wells is attractive where pollution occurs at greater depth, that is, where the construction of PRBs becomes uneconomic. However, the successful field-scale application of any of these techniques as a robust cleanup tool requires good qualitative understanding of the underlying removal mechanisms, and the ability to quantify the physical, chemical, and biological interactions that are involved in the remediation process. One of the key issues that needs to be understood in terms of the robustness of ISMP is the question of how it is affected by potential changes of hydrochemical conditions, and in particular the response to an increasing acidity of the contaminated groundwater. Such a pH decrease can, for example, occur when the aquifer's mineral buffering capacity upstream of the remedial activities becomes depleted [17, 18] and potentially leads to the remobilization of previously immobilized contaminants.

This paper reports the model-based analysis of large-scale laboratory column experiments in which ethanol was used to create favorable conditions for the immobilization of selected trace metals in groundwater. The major objective of the experimental study was to investigate, under well-controlled conditions, the implications of a pH decrease of the metal-contaminated feed solution on the efficiency of the ethanol-driven microbially mediated redox manipulation and on the metal mobility. The numerical modeling study was initiated to support the identification of the major geochemical reactions and to provide a process-based quantification of those reactions, which included the simulation of the dynamic response to increased acidity.

Materials and Methods

Experimental Program. Large-scale soil column experiments were carried out to assess the effectiveness of three different carbon sources (electron donors) in promoting and maintaining favorable conditions for microbially driven sulfate reduction and metal bioprecipitation. Ethanol, molasses, and vegetable oil were tested in the first phase of the project. While all three carbon sources promoted denitrification and copper removal, only the addition of ethanol stimulated sulfate reduction. Therefore the second part of the experiment [20] focused solely on the use of ethanol as an electron donor and carbon source to create reducing conditions. The main focus of those experiments was to assess the effects of a step reduction in the influent groundwater pH from 5.5 to 4.25 on the active bioprecipitation process. For comparison, a control column was operated at the same flow rate without the addition of ethanol. The control column was fed with metal-spiked groundwater, and the pH of the feed solution was changed at the same time as in the ethanol column. Each soil column was constructed from a 2-m-long polyvinyl chloride pipe (15.3 cm i.d.), with 10 sampling ports positioned along the length of the column and with an additional port installed in the delivery line to the column to monitor influent concentrations. The columns were filled with low-sorbing, leached Spearwood sand from the Swan Coastal Plain in

* Corresponding author phone: +61-8-93336272; fax: +61-8-93336211; e-mail: Henning.Prommer@csiro.au.
† CSIRO Land and Water.
‡ University of Western Australia.
§ Current Address: Environmental Resources Management, P.O. Box 266, South Melbourne, VIC, 3205, Australia.

Perth, Western Australia, that had a low total organic carbon content of 200 mg kg^{-1} (dry weight) and a total iron content of 13 mg kg^{-1} (dry weight). Locally (Perth, Western Australia) collected groundwater was spiked with a concentrated metal solution to give a final concentration of 12 mg L^{-1} of Zn and 4 mg L^{-1} of Cu. The solution was acidified with HCl and the pH adjusted to 5.5 for the initial phase of the experiment and to 4.25 thereafter. The soil and groundwater in the columns were used without bioaugmentation. The columns were operated at room temperature (~22 °C), with the influent groundwater flowing upward through the column (from a hydraulic head of 0.5–1 m), controlled by a peristaltic pump on the effluent line to a constant measurable flow of 360 mL day^{-1} (equivalent to a flow velocity of 29 m year^{-1}; assuming a soil porosity of 0.26). A polymer mat, consisting of 5-m-length of silicone tubing (2 mm i.d., 3 mm o.d.) woven through a plastic mesh support frame (13.5 cm diameter), was installed internally 50 cm from the base of the columns. For ethanol delivery to groundwater moving past the tubing weave of the polymer mat in one of the columns, a dilute aqueous ethanol solution (~5−15 g L^{-1} of ethanol) was continuously recycled through the inner volume of the polymer tubing at a rate of 3 mL min^{-1}. Ethanol delivery concentrations to groundwater were ~1 g L^{-1} of ethanol, which was in excess. At 20 weeks after the commencement of ethanol delivery (simulation time = 188 days), when a steady-state redox zonation and metal bioprecipitation had been established for over 10 weeks, the pH of the metal contaminated influent groundwater was decreased from 5.5 to 4.25. Full details on the experimental program can be found in Davis et al. (20).

Numerical Models, Conceptual Model, and Reaction Network. The MODFLOW/MT3DMS-based reactive multi-component transport model PHT3D (21) was used for the reactive transport simulations. PHT3D couples the three-dimensional transport simulator MT3DMS (22) with the geochemical model PHREEQC-2 (23). A conceptual model for the reactive processes within the columns was developed on the basis of the experimental results (20) and subsequently translated into the numerical model by formulating a reaction network of mixed equilibrium and kinetically controlled homogeneous and heterogeneous reactions. During the modeling study, the reaction network was refined stepwise until the numerical model provided a satisfactory description of all observations. To fully account for the observed dynamic changes of the redox zonation, which occurred as a result of microbial lag times, a model formulation that explicitly considered the growth and decay of specific microbial groups was defined. The final reaction network included (i) all major ions; (ii) two organic compounds, ethanol and the trans-formation intermediate acetate; (iii) the microbial groups responsible for the transformation of ethanol and acetate; (iv) the trace metals Zn and Cu; (v) one cation exchanger site for the sorption of cations and hydrogen; and (vi) selected minerals that potentially affected the hydrochemical composition of the aqueous solution. The most important aspects of the reaction network are discussed below.

Modeling of Microbially Mediated Ethanol Degradation. In the numerical model, the ethanol delivered through the polymer mat was assumed to be oxidized in two sequential steps, thereby utilizing oxygen, nitrate, goethite (α-FeOOH), and sulfate as electron acceptors. In the first step, ethanol was transformed to acetate, followed by the second step during which acetate is mineralized. In the model, both steps were assumed to be catalyzed by process-specific microbial degraders. In total, six different groups were included in the simulations, distinguished by (i) the predominant terminal electron-accepting process mediated by each group and (ii) whether the group uses ethanol or acetate as a substrate. Depending on the microbial efficiency of each group, a specific fraction of organic carbon was incorporated into

TABLE 1. Equilibrated Initial Mineral Concentrations and Initial Exchanger Compositions

cations	mol L^{-1}	minerals	mol L$_b^{-1a}$
Ca−X2	1.56×10^{-5}	calcite (CaCO$_3$)	1.00×10^{-4}
Mg−X2	8.39×10^{-6}	goethite (FeOOH)	5.00×10^{-3}
Na−X	9.32×10^{-6}	magnetite	0
K−X	2.93×10^{-6}	FeS (ppt)	0
Fe−X2	0	ZnS (a)	0
Cu−X2	0	Cu Metal (Cu)	0
Zn−X2	0	malachite (Cu$_2$(OH)$_2$CO$_3$)	0
H−X	6.90×10^{-4}		

^{a} Concentrations of minerals in mol L^{-1} of bulk volume.

biomass during microbial growth (24, 25), while the remaining fraction was transformed to acetate (during ethanol degradation) or mineralized to carbon dioxide and water (during acetate degradation). The microbial efficiencies of each group (which influence the stoichiometries of the reactions) were computed following the procedure proposed by Van Briesen and Rittmann (26). A partial equilibrium approach (PEA) (27–32) was employed to incorporate the degradation reactions into the PHT3D/PHREEQC-2 framework. Using the PEA (21, 31) approach, each of the overall degradation reactions (Table SI-1, Supporting Information) is separated into a rate-limiting (i.e., kinetically controlled oxidation step) and into an instantaneous (equilibrium-based) electron-accepting step.

Mineral Dissolution and Precipitation. Mass-balance considerations for several aqueous species, as well as the results from mineral analysis, suggest that a range of mineral dissolution or precipitation reactions proceeded in the experimental columns. During model development, adaptation, and calibration, various likely combinations of mineral reactions were included and tested within the model in order to explain the observed aqueous chemistry. All minerals included in the final reaction network and their initial concentrations are listed in Table 1.

As it was unclear whether the local equilibrium assumption (33) would be valid for the modeled mineral dissolution and precipitation, a kinetic formulation was chosen for all mineral reactions. Following previous modeling studies (12, 13, 34, 35), kinetic rate expressions for most minerals were formulated on the basis of the transition state theory (36):

$$\frac{\partial C}{\partial t} = k_{\text{mineral}} \times (1 - 10^{\text{SI}}) \qquad (3)$$

where A is the surface area of the mineral, k_{mineral} is the rate constant for dissolution, and SI (23) is the saturation index of the mineral. As the mineral surface areas are in our case unknown, the reaction rate constant k_{mineral} is combined with A to yield a single rate constant in the model applications. The rate of calcite dissolution was computed as proposed by Plummer et al. (37) and as included in the standard PHREEQC-2 database (23).

Metal Sorption Reactions. The sorption to an aquifer substrate, and hence mobility of zinc and copper, is strongly influenced by the pH of the groundwater (e.g., 38 and 39). This was confirmed for Cu by a series of batch experiments (Figure SI-4, Supporting Information) carried out prior to the column studies (19). Using the same source of soil and groundwater as in the column studies, the solution pH was varied between 2 and 5.95. The distribution coefficients (K_D) calculated from the observed partitioning varied strongly for Cu within this pH range, while Zn remained largely in solution at this range. Given the spatial and temporal variability of

TABLE 2. Composition of Column Feed Solution before and after the pH Change

aqueous component	column feed solution (ethanol amended column) average values before/ after pH change (mol L^{-1})	aqueous component[a]	column feed solution (ethanol amended column) average values before/ after pH change (mol L^{-1})[a]
pH	5.53/4.24	O(0)	2.00×10^{-4}
pe	n.a.	N(5)[a]	$3.75 \times 10^{-4}/5.24 \times 10^{-4}$
Na	4.15×10^{-3}	N(3),[a] N(0)[a]	0
Cl	5.13×10^{-3}	S(6)[a]	$1.10 \times 10^{-3}/1.20 \times 10^{-3}$
K	2.61×10^{-4}	S(−2)[a]	0
Ca	7.74×10^{-4}	Fe(2)[a]	0
Mg	6.58×10^{-4}	Fe(3)[a]	3.58×10^{-8}
Cu	$7.11 \times 10^{-5}/7.45 \times 10^{-5}$	C(4)[a]	5.32×10^{-4}
Zn	$1.93 \times 10^{-4}/1.86 \times 10^{-4}$	C(−4)[a]	0

[a] Values in brackets indicate valence.

the pH during the column experiment, the partitioning of Cu would not be captured by a simple sorption model such as a linear, single-species, constant K_D sorption model, as routinely used for example to quantify the sorption of nonpolar organic compounds. Therefore, the sorption of copper was incorporated into the model framework through a multicomponent cation exchange model. A similar approach has been previously applied successfully to describe the mobility of cesium (40) across a wide range of concentrations and under strongly varying pH conditions.

In a first step, a single-site model was tested for its ability to describe the data obtained in the batch studies and compared with a two-site and a triple-site model. Hydrogen (H$^+$) was included in all three exchange models to simulate proton buffering reactions. The equilibrium constants for the exchange reactions of Cu and H$^+$ were optimized for the models using the nonlinear parameter optimization program PEST (41). Due to the limited range of experimental data available for the optimization process, the two-site and three-site model performed only marginally better. Therefore, the single-site model (Figure SI-4, Supporting Information) was incorporated into the column models, and the values obtained by this procedure (log K for Cu and log K for H$^+$, Table SI-4, Supporting Information) were used as starting values for the simulations of the column experiments.

Column Feed Solution. The measured water composition of the influent groundwater used in the experiments served as influent boundary conditions for the column. Average concentrations before and after the pH change are listed in Table 2. All significant deviations from the averages were discretized in the model, on the basis of the weekly measurements. Dissolved organic carbon (DOC) was not considered in the simulations as it was assumed that the reactivity of any residual DOC was negligible compared to the reducing capacity of ethanol, and the effect of its mineralization on the water composition in the control column was negligible (19). Before using the measured concentrations as boundary conditions in PHT3D, PHRE-EQC-2 was used in batch simulation mode to investigate whether the measured solution compositions were charge-balanced, with only slight imbalances found. Those were eliminated by adjusting the chloride concentrations.

Model Setup and Discretization. The 2-m-long experimental columns were represented in the numerical model by a one-dimensional domain consisting of 102 grid cells (Figure SI-1, Supporting Information). The effective porosity used for the soil in the column was set to a constant value of 0.26, as determined by a tracer test. It was assumed that neither the formation of biomass nor mineral dissolution or precipitation had significantly altered the porosity over the length of the experiment. The overall simulation period was 546 days. This period was subdivided into daily time steps

to allow the flow rates in the model to be adjusted to the experimentally measured value. The data input for the hydrochemical composition of the column feed solution was discretized into weekly steps, following the availability of chemical analysis of the feed solution. In the experimental column, ethanol was delivered and mixed into the passing groundwater 50 cm from the column base by diffusion through the polymer mat. To reflect this, the measured concentrations from port C (1 cm downstream of the mat) were used as fixed concentrations in the model grid cell that corresponded to the location of the polymer mat. The concentrations of all other components were not fixed at this cell.

Reaction Model Development/Adjustment and Calibration. The reaction network contained a large number of kinetic reactions for which there were many unknown reaction rate constants (parameters) prior to model calibration. However, there are a large number of observations (detailed concentration measurements of a large number of chemicals in space and time) which allowed the model parameters to be constrained successively. Most of the adjustable parameters were required for the microbial model in order to reproduce the dynamic changes in the redox zonation that were observed during the experiment.

In the first phase of the model development and calibration, the estimation of parameters aimed to reproduce the hydrochemical changes in the control column, that is, those changes that occurred in the absence of redox and other reactions triggered by the amendment of ethanol. In the following, the measured nitrate, sulfate, dissolved iron, and acetate concentrations were used as constraints for an initial estimation of the rate-determining parameters of the microbial model. The period before and after the pH change could not be described with a unique set of parameters for the initially defined reaction rate expressions. This was attributed to decreasing microbial growth rates at the lower pH. Therefore a rate dependency on pH was incorporated into the original growth model, which resulted in a good agreement between measured and simulated electron-acceptor concentrations over the entire simulation period. In the last phase of the model development and calibration, the precipitation of Zn- and Cu-bearing minerals was addressed.

Results and Discussion

Mineral Buffering in the Control Column. Observations from the control column and the corresponding model simulations helped identify the processes that occurred in the absence of the ethanol amendment. Two indicators, (i) a slight increase in pH along the length of the column between the start of the experiment and the pH decrease after day 188 and (ii) the slow migration of the low pH front after day 188,
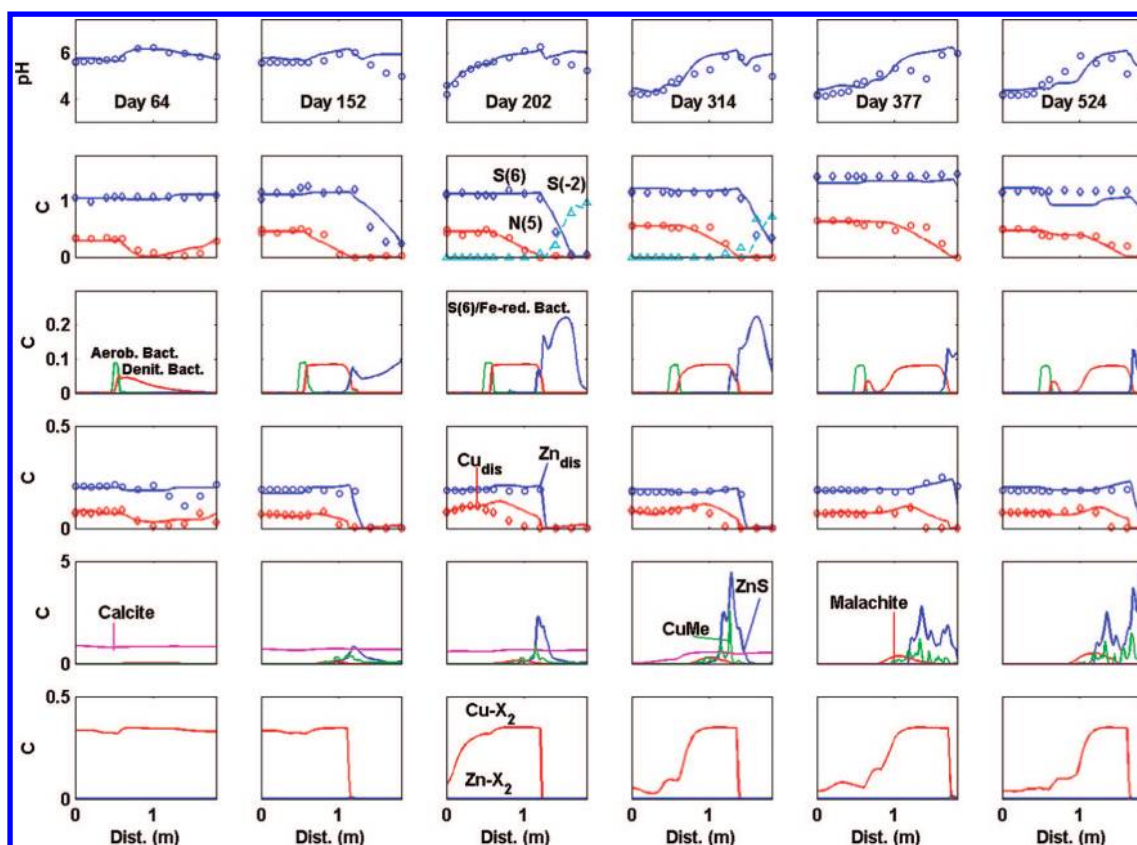
FIGURE 1. Selected concentration profiles at 64, 152, 202, 314, 377, and 524 days after the start of the simulation. Symbols = measured; solid lines = simulated; Zn—X2 = concentrations of Zn sorbed on exchanger X; Cu—X2 = concentrations of Cu sorbed on exchanger X. All aqueous and sorbed concentrations are given in millimoles per liter; mineral concentrations are given in millimoles per liter of bulk volume.

pointed to a buffering effect of mineral reactions. Following the results of X-ray diffraction/X-ray fluorescence (XRD/XRF) analysis (20), calcite was included in the simulations. Both the initial calcite concentration in the column and the reaction rate constant were varied during model calibration. The final model simulations that compared best with the observations suggested that (i) calcite dissolution was controlled by a kinetic reaction (where calcite was available) and (ii) a calcite-depleted zone started to form near the column entry soon after the pH in the feed solution was decreased. Given the natural heterogeneity of soils, the model-determined initial calcite concentration (1.0×10^{-4} mol L_b^{-1}) agreed well with the value measured by quantitative XRD (5.3×10^{-5} mol L_b^{-1}). Approximately 400 days after the start of the simulation, the modeled low-pH front reached the column exit when calcite was depleted throughout the entire column. This modeled spatial and temporal evolution of the pH agrees well with the measured data (Figure SI-2, Supporting Information).

Zn and Cu Mobility in the Control Column. To identify the role of ethanol amendment on metal mobility, the feed solution of the control columns contained similar Zn and Cu concentrations as the ethanol amended column. After a lag period, Zn and Cu concentrations at the column effluent end were similar to those in the feed solution. This can be interpreted as an indication that no significant precipitation reactions of either Zn- or Cu-bearing minerals had occurred in the control column, while the observed retardation suggests the occurrence of (reversible) sorption/exchange reactions. In the case of Zn, effluent concentrations remained stable over the duration of the experiment, and the pH decrease in the feed solution had essentially no effect on the dissolved concentrations of Zn. This confirmed the results from the batch tests, which also indicated that, for the pH

range prevailing in the control columns, Zn mobility would not be significantly affected by precipitation reactions. In contrast, dissolved Cu concentrations were affected by the pH decrease of the feed solution. The concentrations of dissolved Cu increased immediately after the pH decrease to concentration levels above the influent concentration. This behavior, which results from the desorption of Cu, was well captured by the cation exchange model included in the simulations. However, good results were only obtained once the equilibrium constants for the exchange reactions of Cu and H^+ had been further modified relative to those obtained for the batch experiments (Figure SI-2 and Table SI-4, Supporting Information).

Redox Zonation in the Ethanol Amended Column before the pH Decrease. The model built for the control column simulation, including the processes that were identified (mineral buffering and Cu sorption/ion exchange), was used as a base for the simulation of the ethanol-amended column experiment. In the simulation period before the pH change (day 0—188), the redox chemistry was characterized by dynamic changes in the initial phase after ethanol amendment commenced (approximately day 50—100), followed by a more stable redox zonation until day 188. The model simulates the microbial lag period of approximately 12 days from the start of ethanol delivery and the time when denitrifying conditions were established (Figure 1). Where nitrate became depleted, dissolved iron concentrations started to increase, indicating the onset of iron reduction. Sulfate reduction started to occur significantly later, only from day 98 on. The model was able to reproduce this sequence of microbially mediated redox processes. However, the maintenance of iron reduction in the model over an extended period, without the onset of sulfate reduction, was only possible when kinetically controlled magnetite (Fe_3O_4)

precipitation was included in the simulation. Without the inclusion of magnetite, a rapid pH increase occurred during iron reduction, causing an immediate shift in electron-acceptor consumption to sulfate. For the model, it was assumed that only a limited amount of bioavailable iron (as goethite, FeOOH) was present and that rates would decrease with progressing depletion of the goethite.

Under aerobic, denitrifying, and iron-reducing conditions, the rate constants for the mineralization reactions of acetate were set high enough to prevent a significant accumulation of acetate. In contrast, for sulfate-reducing conditions, the modeled acetate concentrations only agreed with the measured values if no or only a very slow mineralization of acetate was assumed.

Inhibitory Effect of Acidity on Microbial Activity and Corresponding Changes in Redox Zonation. The decrease of pH after day 188 had initially (for the first few weeks after the pH change) no effect on the redox zonation. During the model calibration, a good match between simulated and observed electron-acceptor concentrations was therefore possible with the same microbial model parametrization as for the period before the pH change. However, with progressing simulation time, an increasing discrepancy between model results and experimental observations was found to occur as the low pH zone migrated successively further along the column, where calcite had become depleted. This was interpreted as an inhibitory effect of the acidity on the microbial activity (e.g., *42*). To accommodate this effect in the numerical model, the original model formulation for microbial growth was extended by an inhibition term proposed by Winter et al. (*43*):

$$I_{pH} = \frac{k_{pH}}{(k_{pH} + 10^{|\mu pH - pHI|})} - 1 \quad (4)$$

where k_{pH} is an inhibition factor and pH is the pH of optimum growth conditions. The inhibition term in eq 4 has been previously used for biogeochemical transport modeling, for example, for a landfill leachate contamination in Denmark (*44*). The effect of k_{pH} on the value of the inhibition term I_{pH} is illustrated in Figure SI-5 (Supporting Information). After the incorporation of the term, a good agreement between measured and simulated electron-acceptor concentrations was achieved. The model was able to capture the successive downstream migration of the denitrifying zone and the complete disappearance of the sulfate-reducing zone. Thus, the presence of the buffering mineral calcite and its successive depletion had a controlling effect on the redox zonation within the column.

Zn Mobility in the Ethanol Column. Zinc immobilization in the experimental columns proceeded rapidly where redox conditions switched from denitrifying to sulfate-reducing conditions. In the model, this immobilization was well captured in space and time by the inclusion of amorphous ZnS (see Figure 1). This confirms the feasibility of in situ zinc removal by ethanol amendment. However, with the successive disappearance of sulfate-reducing conditions within the column under reduced pH conditions, zinc removal by the precipitation of ZnS ceased. Moreover, dissolved Zn concentrations increased to concentrations above that in the feed solution. The model was able to reproduce this effect very well.

Cu Mobility in the Ethanol Column. In contrast to Zn, the immobilization of Cu in the ethanol-amended columns occurred earlier along the column length under denitrifying conditions, that is, in the absence of sulfate-reducing conditions. The initial hypothesis that was tested in the model was that elemental Cu (Cu-metal) would potentially precipitate within the denitrifying zone as a result of the lowered redox potential relative to the redox-potential of the feed solution. While elemental Cu indeed formed during the model simulations, oversaturation and/or precipitation occurred only at locations downstream of where redox conditions have switched from denitrification to sulfate reduction. However, malachite ($Cu_2(OH)_2CO_3$) became in the simulations over-saturated and/or formed already within the denitrifying zone where carbonate was produced during ethanol mineralization. As in the control column, increased dissolved Cu concentrations occurred in response to the pH decrease of the feed solution. The model reproduced this effect as a result of Cu desorption from the cation-exchange sites. The modeled Cu concentration is shown in Figure 1 in comparison with measured concentration. The figure also shows the modeled concentrations of selected minerals (calcite, amorphous ZnS, Cu-metal, and malachite), as well as the concentrations of sorbed Cu and Zn.

Role of Modeling for the Determination of Metal Remediation Performance. The reactive transport modeling study demonstrates the complex interdependency of the geochemical and microbiological processes that govern the fate of the trace metals during remediation by carbon amendment. The accurate simulation of the observed dynamic geochemical changes, including the metal fate, required the incorporation of a relatively detailed model of microbial activity. The modeling results show that mineral buffering plays a key role in maintaining the remedial efficiency of the bioprecipitation process. In the absence of neutralization reactions and at the resulting lower pH of the aqueous solution, the microbial efficiency was significantly decreased. The model simulations were an important tool for the identification of the conceptual model. They provide now a process-based explanation and quantification of (i) the temporally changing redox zonation, (ii) the resulting effects on the metal bioprecipitation processes, and (iii) the observed remobilization of Cu and Zn that occurred after the decrease of the pH in the feed solution. Clearly, some uncertainty remains in the model-based interpretation of such complex processes (*12, 31*), in particular where measured data that underpin the proposed conceptual model are unavailable (e.g., microbial concentrations) or not available at the required density.

Supporting Information Available

Additional figures and tables and the model's reaction database are available. This material is available free of charge via the Internet at http://pubs.acs.org.

Literature Cited

(1) Gillham, R. W. Cleaning Halogenated Contaminants from Groundwater. U.S. Patent No. 5,266,213, 1993.

(2) Gillham, R. W.; O'Hannesin, S. F. Enhanced degradation of halogenated aliphatic by zero-valent iron. *Ground Water* **1994**, *32* (6), 958–967.

(3) Benner, S. G.; Blowes, D. W.; Ptacek, C. J. A full-scale porous reactive wall for prevention of acid mine drainage. *Ground Water Monit. Rem.* **1997**, *17* (4), 99–107.

(4) Benner, S. G.; Blowes, D. W.; Gould, W. D.; Herbert, R. B., Jr.; Ptacek, C. J. Geochemistry of a permeable reactive barrier for metals and acid mine drainage. *Environ. Sci. Technol.* **1999**, *33* (16), 2793–2799.

(5) Blowes, D. W.; Ptacek, C. J.; Benner, S. G.; McRae, C. W.; Bennett, T. A.; Puls, R. W. Treatment of inorganic contaminants using permeable reactive barriers. *J. Contam. Hydrol.* **2000**, *45* (1–2), 123–137.

(6) Waybrant, K. R.; Blowes, D. W.; Ptacek, C. J. Selection of reactive mixtures for use in a permeable reactive wall for the treatment of mine drainage. *Environ. Sci. Technol.* **1998**, *32* (13), 1972–1979.

(7) Doerr, N. A.; Ptacek, C. J.; Blowes, D. W. Effects of a reactive barrier and aquifer geology on metal distribution and mobility in a mine drainage impacted aquifer. *J. Contam. Hydrol.* **2006**, *78* (1–2), 1–25.

(8) Diels, L.; van der Lelie, N.; Bastiaens, L. New developments in treatment of heavy metal contaminated soils. *Rev. Environ. Sci. Biotechnol.* **2002**, *1* (1), 75–82.

(9) Amos, P. W.; Younger, P. L. Substrate characterisation for a subsurface reactive barrier to treat colliery spoil leachate. *Water Res.* **2003**, *37* (1), 108–120.

(10) Janssen, G. M. C. M.; Temminghoff, E. J. M. In situ metal precipitation in a zinc-contaminated, aerobic sandy aquifer by means of biological sulfate reduction. *Environ. Sci. Technol.* **2004**, *38* (14), 4002–4011.

(11) Tsukamoto, T. K.; Killion, H. A.; Miller, G. C. Column experiments for the microbiological treatment of acid mine drainage: low-temperature, low pH and matrix investigations. *Water Res.* **2004**, *38* (6), 1405–1418.

(12) Amos, R. T.; Mayer, K. U.; Blowes, D. W.; Ptacek, C. J. Reactive transport modeling of column experiments for the remediation of acid mine drainage. *Environ. Sci. Technol.* **2004**, *38*, 3131–3138.

(13) Mayer, K. U.; Benner, S. G.; Blowes, D. W. Process-based reactive transport modeling of a permeable reactive barrier for the treatment of mine drainage. *J. Contam. Hydrol.* **2006**, *85* (3–4), 195–211.

(14) Patterson, B. M.; Grassi, M. E.; Davis, G. B.; Robertson, B.; McKinley, A. J. Use of polymer mats for sequential reactive barrier remediation of ammonium-contaminated groundwater: laboratory column evaluation. *Environ. Sci. Technol.* **2002**, *36* (15), 3439–3445.

(15) Patterson, B. M.; Grassi, M. E.; Robertson, B.; Smith, A. J.; Davis, G. B.; McKinley, A. J. The use of polymer mats in series for sequential reactive barrier remediation of ammonium-contaminated groundwater: field evaluation. *Environ. Sci. Technol.* **2004**, *38*, 6846–6854.

(16) Diels, L.; van der Lelie, D.; Gemoets, J.; Springael, D.; Geets, J.; Vos, J.; Bastiaens, L. In situ bioprecipitation of heavy metals in groundwater. In *Biohydrometallurgy: Fundamentals, Technology and Sustainable Development*; Ciminelli, V. S. T., Garcia Jr., O., Eds.; Elsevier Science: New York, 2001; Process Metallurgy Series, Vol. 11B, pp 503–511.

(17) Walter, A. L.; Frind, E. O.; Blowes, D. W.; Ptacek, C. J.; Molson, J. W. Modeling of multicomponent reactive transport in groundwater. 1. Model development and evaluation. *Water Resour. Res.* **1994**, *30* (11), 3137–3148.

(18) Bain, J. G.; Mayer, K. U.; Blowes, D. W.; Frind, E. O.; Molson, J. W. H.; Kahnt, R.; Jenk, U. Modelling the closure-related geochemical evolution of groundwater at a former uranium mine. *J. Contam. Hydrol.* **2001**, *52*, 109–135.

(19) Davis, A. C. Effects of acidity on bacterial sulfate reduction and metal bioprecipitation in acid rock drainage groundwater using three different carbon sources. Unpublished Masters Thesis, Faculty of Life and Physical Sciences, University of Western Australia, 2005.

(20) Davis, A. C.; Patterson, B. M.; Grassi, M. E.; Robertson, B. S.; Prommer., H.; McKinley, A. J. The effects of increasing acidity on metal(loid) bioprecipitation in groundwater: Column studies. *Environ. Sci. Technol.* **2007** (accepted for publication).

(21) Prommer, H.; Barry, D. A.; Zheng, C. MODFLOW/MT3DMS based reactive multi-component transport model. *Ground Water* **2003**, *41* (2), 247–257.

(22) Zheng, C.; Wang, P. P. *MT3DMS: A modular three-dimensional multispecies model for simulation of advection, dispersion and chemical reactions of contaminants in groundwater systems-*;Documentation and User's Guide, Contract Report SERDP-99-1, U.S. Army Engineer Research and Development Center: Vicksburg, MS, 1999.

(23) Parkhurst, D. L.; Appelo, C. A. J. *User's guide to PHREEQC - A computer program for speciation, reaction-path, 1D-transport, and inverse geochemical calculations, 99-4259*; U.S. Geological Survey Water-Resources Investigations Report, U.S. Geological Survey: Washington, DC, 1999.

(24) Rittmann, B. E.; VanBriesen, J. M. Microbiological processes in reactive modelling. In *Reactive Transport in Porous Media*; Lichtner, P. C., Steefel, C. I., Oelkers, E. H., Eds.; Mineralogical Society Of America: Chantilly, VA, 1996; pp 311–334.

(25) Prommer, H.; Barry, D. A. Modeling Bioremediation of Contaminated Groundwater. *Bioremediation*; Atlas, R. M., Philp, J., Eds.; American Society for Microbiology: Washington, DC, 2005.

(26) VanBriesen, J. M.; Rittmann, B. E. Mathematical description of microbial reactions involving intermediates. *Biotechnol. Bioeng.* **2000**, *67* (1), 35–52.

(27) Postma, D.; Jakobsen, R. Redox zonation: equilibrium constraints on the Fe(III)/SO4-reduction interface. *Geochim. Cosmochim.* **1996**, *60*, 3169–3175.

(28) Jakobsen, R.; Postma, D. Redox zoning, rates of sulfate reduction, and interactions with Fe-reduction and methanogenesis in a shallow sandy aquifer, Rømø, Denmark. *Geochim. Cosmochim.* **1999**, 137–151.

(29) Brun, A.; Engesgaard, P. Modelling of transport and biogeochemical processes in pollution plumes: Model formulation and development. *J. Hydrol.* **2002**, *256*, 211–227.

(30) Prommer, H.; Barry, D. A.; Davis, G. B. Influence of transient groundwater flow on physical and reactive processes during biodegradation of a hydrocarbon plume. *J. Contam. Hydrol.* **2002**, *59*, 113–132.

(31) Greskowiak, J.; Prommer, H.; Vanderzalm, J.; Pavelic, P.; Dillon, P. Modelling of carbon cycling and biogeochemical changes during a wastewater injection and recovery experiment at Bolivar/South Australia. *Water Resour. Res.* **2005**, *41*. DOI: 10.1029/2005WR004095.

(32) Greskowiak, J.; Prommer, H.; Massmann, G; Nützmann, G. Modelling the seasonally changing fate of the pharmaceutical residue phenazone during artificial recharge of groundwater. *Environ. Sci. Technol.* **2006**, *40* (21), 6615–6621.

(33) Bahr, J. M.; Rubin, J. Direct comparison of kinetic and local equilibrium formulations for solute transport affected by surface reactions. *Water Resour. Res.* **1987**, *23* (3), 438–452.

(34) Yabusaki, S.; Cantrell, K.; Sass, B.; Steefel, C. Multicomponent reactive transport in an in situ zero-valent iron cell. *Environ. Sci. Technol.* **2001**, *35*, 1493–1503.

(35) Mayer, K. U.; Blowes, D. W.; Frind, E. O. Reactive transport modelling of groundwater remediation by an in-situ reactive barrier for the treatment of hexavalent chromium and trichloroethylene. *Water Resour. Res.* **2001**, *37*, 3091–3103.

(36) Lasaga, A. C. *Kinetic Theory in the Earth Sciences*; Princeton University Press: Princeton, NJ.

(37) Plummer, L. N.; Wigley, T. M. L.; Parkhurst, D. L. The kinetics of calcite dissolution in CO2-water systems at 5 to 60 C and 0.0 to 1.0 atm CO2. *Am. J. Sci.* **1978**, *278*, 179–216.

(38) Davis, J. A.; Kent, D. B. Surface complexation modeling in aqueous geochemistry. In *Mineral-Water Interface Geochemistry*; Hochella, M. F., White, A. F., Eds.; Mineral Society of America: Washington, DC, 1990; Rev. Mineral. Ser., pp. 177–260.

(39) Kent, D. B.; Abrams, R. H.; Davis, J. A.; Coston, J. A.; LeBlanc, D. R. Modeling the influence of variable pH on the transport of zinc in a contaminated aquifer using semiempirical surface complexation models. *Water Resour. Res.* **2000**, *36*, 3411–3425.

(40) Steefel, C. I.; Carroll, S.; Zhao, P.; Roberts, S. Cesium migration in Hanford sediment: a multisite cation exchange model based on laboratory experiments. *J. Contam. Hydrol.* **2003**, *67*, 219–246.

(41) Doherty, J. *PEST - Model-Independent Parameter Estimation. User's Manual*, 5th ed.; Watermark Numerical Computing: Brisbane, Australia, 2002.

(42) Rosso, L.; Lobry, J. R.; Bajard, S.; Flandrois, J. P. Convenient Model To Describe the Combined Effects of Temperature and pH on Microbial Growth. *Appl. Environ. Microbiol.* **1993**, *61* (2), 610–616.

(43) Winter, L.; Linde-Jensen, J. J.; Mikkelsen, I.; Jensen, T. H.; Henze, M. *Spildevandsteknik.* (in Danish); Polytekinsk Forlag: Denmark, 1978.

(44) Brun, A. Reactive transport modeling of coupled inorganic and organic processes in groundwater. Ph.D. Thesis, Department of Hydrodynamics and Water Resources, Technical University of Denmark, Lyngby, Copenhagen, Denmark, 1998.